J. Min. Metall. Sect. B-Metall. 58 (1) (2022) 157 - 167

Journal of Mining and Metallurgy, Section B: Metallurgy

# MICROSTRUCTURE AND MECHANICAL PROPERTIES OF A7N01 ALUMINUM ALLOY WELD JOINTS FILLED WITH ER5356 AND ER5087 WELD WIRES

**H. Xie *, L. Hu, Q.-H. Ma, W. Meng, X.-H. Yin**

School of Materials Science and Engineering, Anhui University of Technology, Ma'anshan, Anhui, China

*(Received 25 June 2021; Accepted 24 December 2021)*

***Abstract:***

*The A7N01-T5 aluminum alloy plates with the thickness of 12 mm were welded with the ER5356 and ER5087 welding wires, respectively, by the method of Metal Inert Gas (MIG) welding. The mechanical properties and microstructures of the welded joints were investigated by micro-hardness measurement, tensile test, energy dispersive spectroscopy (EDS), electron backscattered diffraction (EBSD) and transmission electron microscopy (TEM). The results showed that the tensile strength and elongation of 7N01/5087 welded joint (the 7N01 aluminum alloy plate welded with ER5087 wire) were greater than those of 7N01/5356 welded joint (the 7N01 aluminum alloy plate welded with ER5356 wires), respectively. The high strength and the good elongation of 7N01/5087 welded joint were mainly attributed to the microstructure refinement in the weld zone through adding Zr element to promote the nucleation of Al grains around the $Al_3Zr$ sites.*

***Keywords:*** *Aluminum alloys; ER5087 welding wire; ER5356 welding wire; Microstructure; Mechanical properti*es

## 1. Introduction

The Al-Zn-Mg alloys were extensively used as structural material in industries, and application ranged from high-speed train body to cryogenic pressure vessels [1-5]. As a typical Al-Zn-Mg alloy, the A7N01 aluminum alloy had good welding performance, excellent corrosion resistance and strength [6]. Hence, the A7N01 alloy was being increasingly used for the high-speed train body structures.

Welding was the primary method used to join aluminum alloy structures because it could decrease the high manufacturing cost and simplify product design [7-10]. Hence, the welding of 7N01 aluminum alloy plates has attracted many interests in recent years due to its importance. Wang et al. [11] used laser-arc hybrid with ER5356 wire to weld the 7N01 aluminum alloy plate, and found that the weld joint had both low residual stress and excellent mechanical properties. He also pointed out that the fusion zone possessed the lowest microhardness and tensile strength, mainly because of its as-cast structure with equiaxed grains and coarse particles. Zhang et al. [12] investigated the effect of the welding thermal cycle on the softening and aging behaviors of the 7N01 aluminum alloy by examining the state of the strengthening precipitates. He found that the softening behavior of the aluminum alloys was closely related to the volume fraction and size of the hardening precipitates, which were greatly affected by the peak temperature of the welding thermal cycle.

For the welding of aluminum alloy in high-speed train body, metal-inert-gas (MIG) welding was a conventional and preferred fusion-welding technology because it was applicable, economical and efficient [13-15]. As a commercial aluminum alloy wire, ER5356 wire was widely used in the high-speed train body welding. However, the mechanical property of the welded joint filled with ER5356 wire was out of ideal and the joint was also susceptible to heat cracking due to the coarse solidified grains in the weld zone [16]. Hence, it is necessary to find a new welding wire instead of the original ER5356 welding wire. Unfortunately, little research work has been devoted to this issue.

The addition of rare earth elements into welding wire was a good choice to improve the weld properties of the weld joint [17-19]. Huang et. al[20] carried out TIG welding to 7A52 aluminum alloy sheets, using ER5356 welding wires with Sc and without Sc, respectively. The yield strength and elongation of the welded joint welded by Sc-added ER5356 wire were 24% and 37% higher than that by ER5356 wire without Sc, respectively. However, for the welding of aluminum alloy in the high-speed train body, the amount of welding wire required for each

* *Corresponding author: 979957762@qq.com*

***https://doi.org/10.2298/JMMB210625056X***

carriage was very large [21]; the weld seam of each carriage was 2.5 kilometers long and 500kg of welding wire was required. Hence, the high production cost made it difficult to employ the extensive commercial application of Sc-added welding wire to weld the high-speed train body. As a Zr-added wire, the ER5087 wire had good compatibility with the base metal, and the relatively low price also ensured extensive application in train's body welding. Thus, the ER5087 wire had great potential to replace the existing ER5356 wire in the welding of high-speed train body. For better understanding, the literature survey of the welding of Al-Zn-Mg aluminum alloy was listed in Table 1.

In this paper, MIG welding was applied on A7N01 aluminum alloy plate, using ER5087 and ER5356 alloy as filler materials, respectively. Based on this, the microstructures and mechanical properties of the weld joints filled with ER5087 and ER5356 welding wires were studied comparatively. The finding of this paper was to explore a new welding wire to weld the high-speed train body with advanced mechanical properties.

## 2. Experimental procedure

### *2.1. Materials*

The materials used in this study was A7N01 aluminum alloy plate aged artificially (T5), with the thickness of 12mm. The chemical composition of the A7N01 and the welding wires are listed in Table 2.

### *2.2. MIG welding process*

Manual MIG welding was conducted on a Fronius VR4000 MIG welding machine at China Aerospace Research Institute of Materials Processing & Technology, and the filler materials were ER5356 and ER5087 welding wires, respectively. The welding wires were supplied by Atlantic welding materials Co., Ltd., with a diameter of 1.2mm. The surface of base-metal and the welding wires were cleaned by ethyl alcohol before welding. "V-shape" groove was made by milling with 70°groove angle, and the root face was 2mm. Welding process was divided into four layers and there were six weld beads in total. The schematic diagram of the welding groove and the distribution of welding beads were shown in Figure 1. Meanwhile, the parameters of MIG welding were shown in Table 3.

### *2.3. Mechanical test and microstructure observation*

Vickers micro-hardness measurements were carried out on HVS-1000 digital Vickers micro-hardness tester, with a load of 0.1kg and a dwell time of 10 s at 2 mm intervals. Two positions on the cross-section of the 7N01/5356 welded joint and the 7N01/5087 welded joint, including the bottom and top positions, were tested. Fig. 3(a) showed the exact positions of the test lines. The tensile testing was performed at room temperate on a MTS810 universal testing machine with a tensile velocity of 2mm/min. All test data were obtained by three parallel samples. Fig. 2 showed the sampling locations of the tensile specimens for the welded plates.

The elements content was measured through X-ray energy disperse spectroscopy (EDS) analysis on a Quanta MK2-200 scanning electron microscope (SEM). Electron backscattered diffraction (EBSD,

***Table 1.*** *Literature survey of the welding of Al-Zn-Mg alloy*

| Research projects | Contents | Conclusions | Remarks |
|---|---|---|---|
| New welding method | Laser-arc hybrid welded with ER5356 wire | Both low residual stress and excellent mechanical properties | |
| Microstructure analysis of the weld joint | The welding thermal cycle on the softening and aging behaviors of the weld joint | The peak temperature of the welding thermal cycle affects the size and volume of the precipitates, resulting in the softening of the weld joint | |
| Improvement of the weld wire | Comparative study of the microstructure and mechanical properties of the weld joints filled with ER5356 and Sc-added ER5356 weld wires | The addition of Sc into the weld wire effectively improves the mechanical properties of the weld joint | The high cost limits the extensive commercial application of Sc-added weld wire |

***Table 2.*** *Compositions of base metal and welding wires*

| Materials | Chemical compositions (weight %) | | | | | | | | | |
|---|---|---|---|---|---|---|---|---|---|---|
| | Zn | Mg | Cu | Mn | Cr | Zr | Ti | Fe | Si | Al |
| A7N01 | 4.35 | 1.5 | 0.15 | 0.34 | 0.20 | 0.18 | 0.09 | 0.08 | 0.06 | Bal. |
| ER5356 | — | 5.1 | — | 0.01 | 0.07 | — | 0.05 | — | — | Bal. |
| ER5087 | — | 5.0 | — | 0.8 | 0.08 | 0.15 | 0.12 | — | — | Bal. |

Sirion 200) was used to study the grain boundary characteristics in different zones of the welded joints. The thin foils for transmission electron microscopy (TEM) were polished by a MTP-II twin-jet polishing with an electrolyte consisting of 70% methanol and 30% nitric acid at -25°C. The foils were observed on a TECNAI G2 20 transmission electron microscope.

## 3. Results and discussion

### *3.1. Micro-hardness distribution of welded joints*

Fig.3 showed the cross-sectional morphologies of the two welded joints and the microhardness profiles across the samples. It could be seen that there was no-macro-level crack, porosity, or other defects in the joints, indicating that both the welding wires had good compatibilities with the 7N01 base metal. The widths of the top and the bottom of the weld zone were about 10mm and 4mm, respectively. For the two welded joints, the distribution of micro-hardness was symmetrical about the welding center line. The minimum value of micro-hardness located in the weld zone and the hardness in the heat-affected zone was also quite low. The hardness value of the welded joint filled with ER5087 welding wire (85-95HV) was about 12% higher than that of 7N01/5356 welded joint (75-82HV) on the whole.

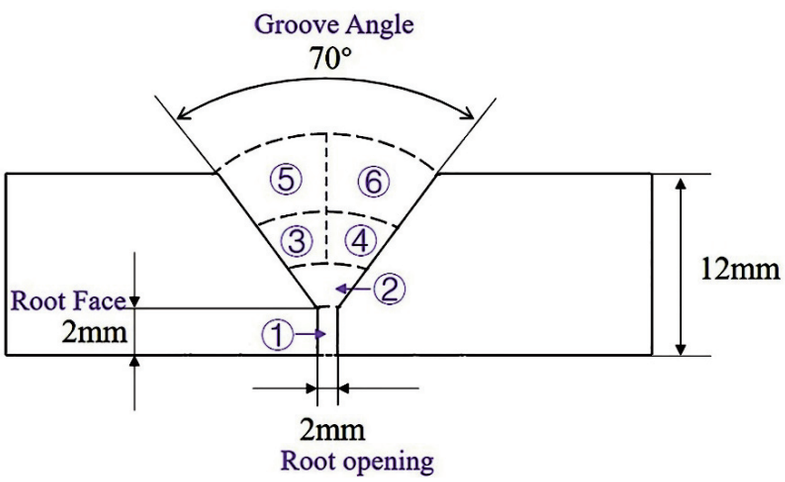


***Figure 1.*** *Schematic diagram of the welding groove and the distribution of welding beads*

***Table 3.*** *Parameters of MIG welding*

| Weld bead No. in Fig.1 | Weld method | Current/A | Voltage/V | Flow rate/(l/min) | Welding speed/(mm/sec) |
|---|---|---|---|---|---|
| 1 and 2 | Rooting weld | 246 | 23.5 | 20-25 | 7.5 |
| 3 and 4 | Filling weld | 262 | 23.1 | 20-25 | 8.0 |
| 5 and 6 | Capping weld | 275 | 24.2 | 20-25 | 8.5 |

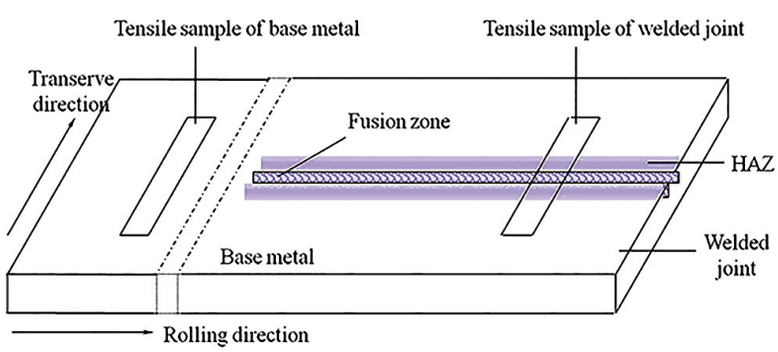


***Figure 2.*** *Schematic illustration of the specimen sampling*

### 3.2. Tensile property

The tensile properties of the welded joints using ER5087 and ER5356 as filler materials were shown in Fig.4. The fracture positions of all the specimens were in the weld zone. Compared with 7N01/5356 welded joint, the average strength and elongation of 7N01/5087 welded joint were higher: the ultimate strength, yield strength and elongation of 7N01/5087 welded joint were 320 MPa, 186 MPa and 6.4%, respectively, while those of 7N01/5356 welded joint were 288 MPa, 176 MPa and 4.9%, respectively.

### 3.3. Microstructures of the welded joints

#### 3.3.1. EBSD images of the welded joints

Fig.5 showed the EBSD images of base metal and welding joints. MIG welded joints could be subdivided into four microstructure zones: base metal (BM), heat-affected zone (HAZ), fusion zone (FZ), and weld zone (WZ). The microstructure of base metal was fibrous and elongated along the rolling direction with a small amount of recrystallized grains (Fig. 5a). The grain sizes of the 7N01/5356 weld zone were concentrated in the distribution of 30-65μm (Fig. 5d and e), which was much larger than those of the 7N01/5087 weld zone with the grain sizes of about 5-25μm (Fig. 5b and c). The weld zone and the fusion zone were both well bonded, and the microstructure of fusion zone was coarse columnar crystals (Fig. 5f and g).

#### 3.3.2. Energy disperse spectroscopy (EDS) of the two welded joints

Fig.6 showed the EDS results of the two welded joints. The elements of the 7N01/5087 weld zone were essentially the same as those of the ER5087 welding wire. Moreover, the 7N01/5087 weld zone containing Zr element, and Mn element was significantly higher than that of 7N01/5356 weld zone (Fig. 6c and d).

#### 3.3.3. TEM images of the welded joints

Fig.7 showed the bright filed TEM images of the weld zone of the two welded joints. The grains in the weld zone of the two welded joints were similar to the single-phase solid solution (Fig. 7a and c). Compared with the 7N01/5356 welded joint, $Al_3Zr$ particles were

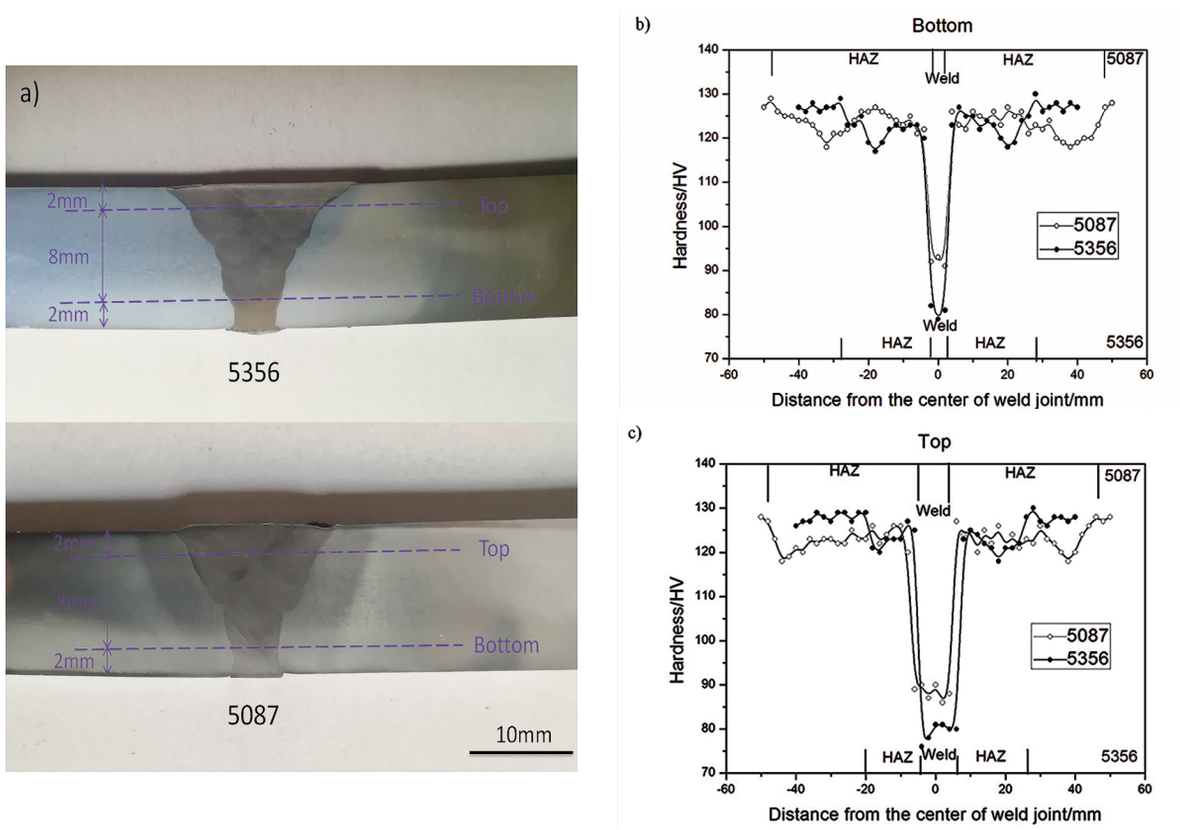


***Figure 3.*** *Cross-sectional morphologies of the two welded joints and microhardness profiles across the samples: a) cross-sectional morphologies of the two weld joints and microhardness profiles measurement positions; b) microhardness profile at the bottom position of the welded joint; c) microhardness profile at the top position of the welded joint*

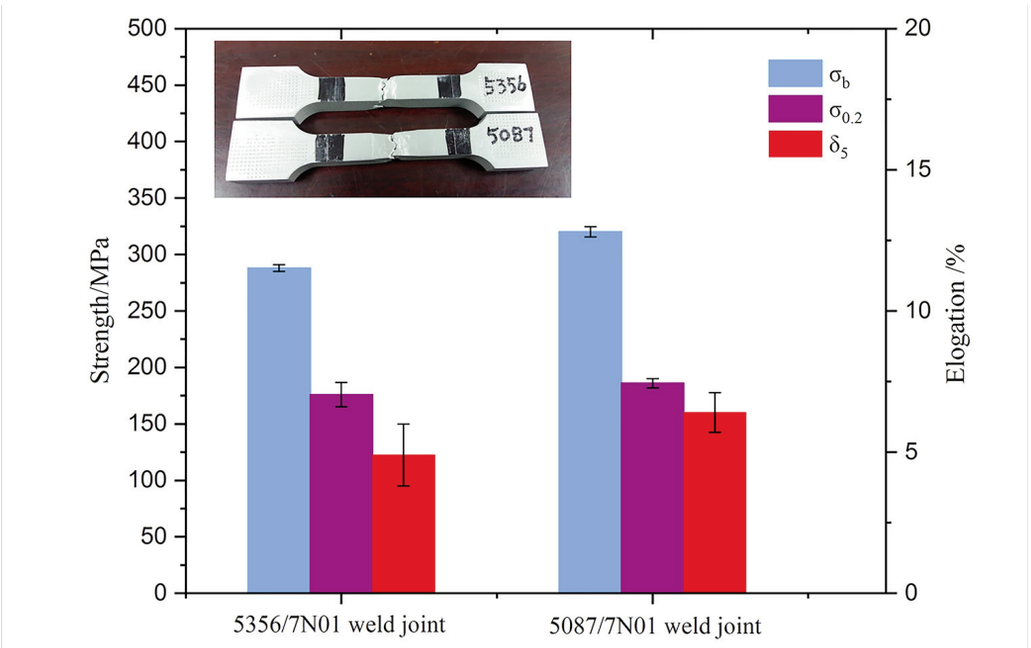


***Figure 4.*** *Tensile mechanical properties of the welded joints*

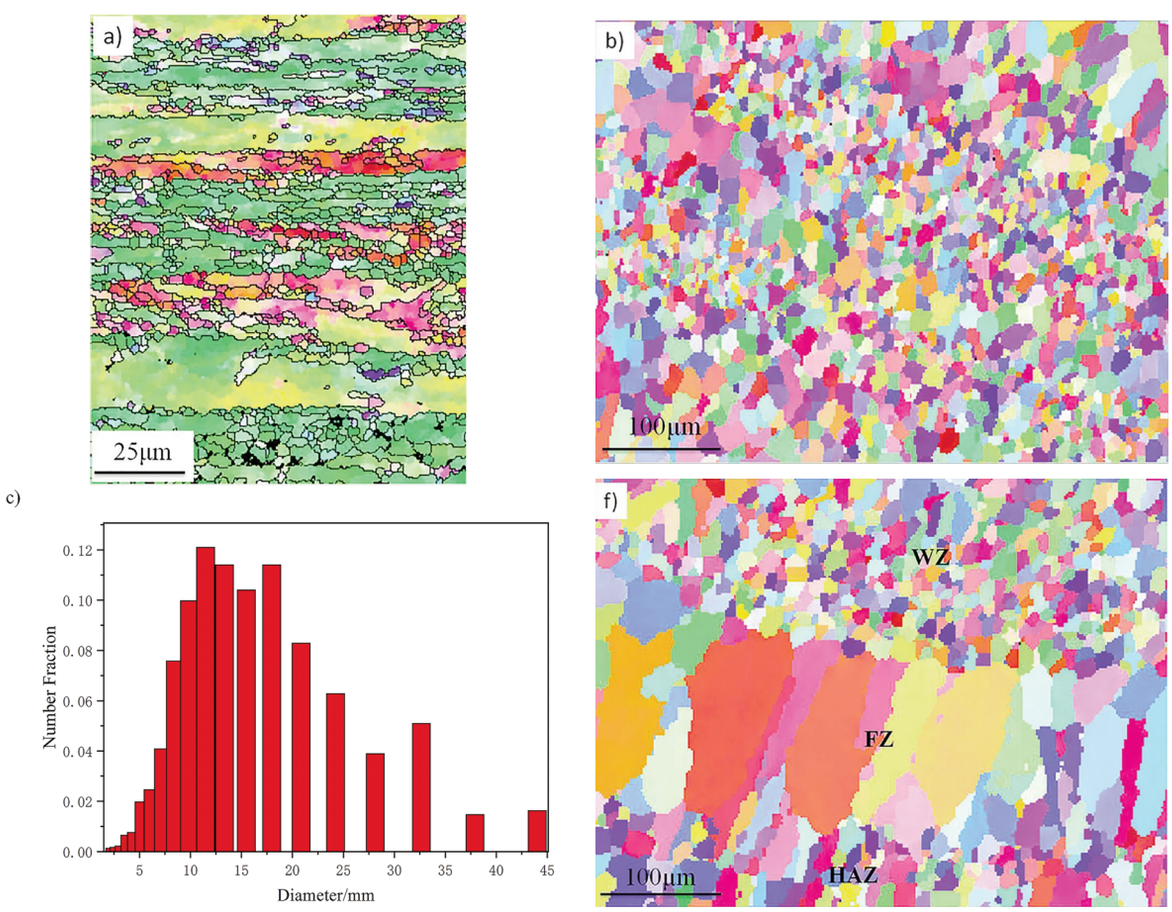


***Figure 5.*** *EBSD images of the two welded joints: a) base metal; 7N01/5087 welded joint: b) weld zone, c) grain size distribution image of the weld zone, f) fusion zone;*

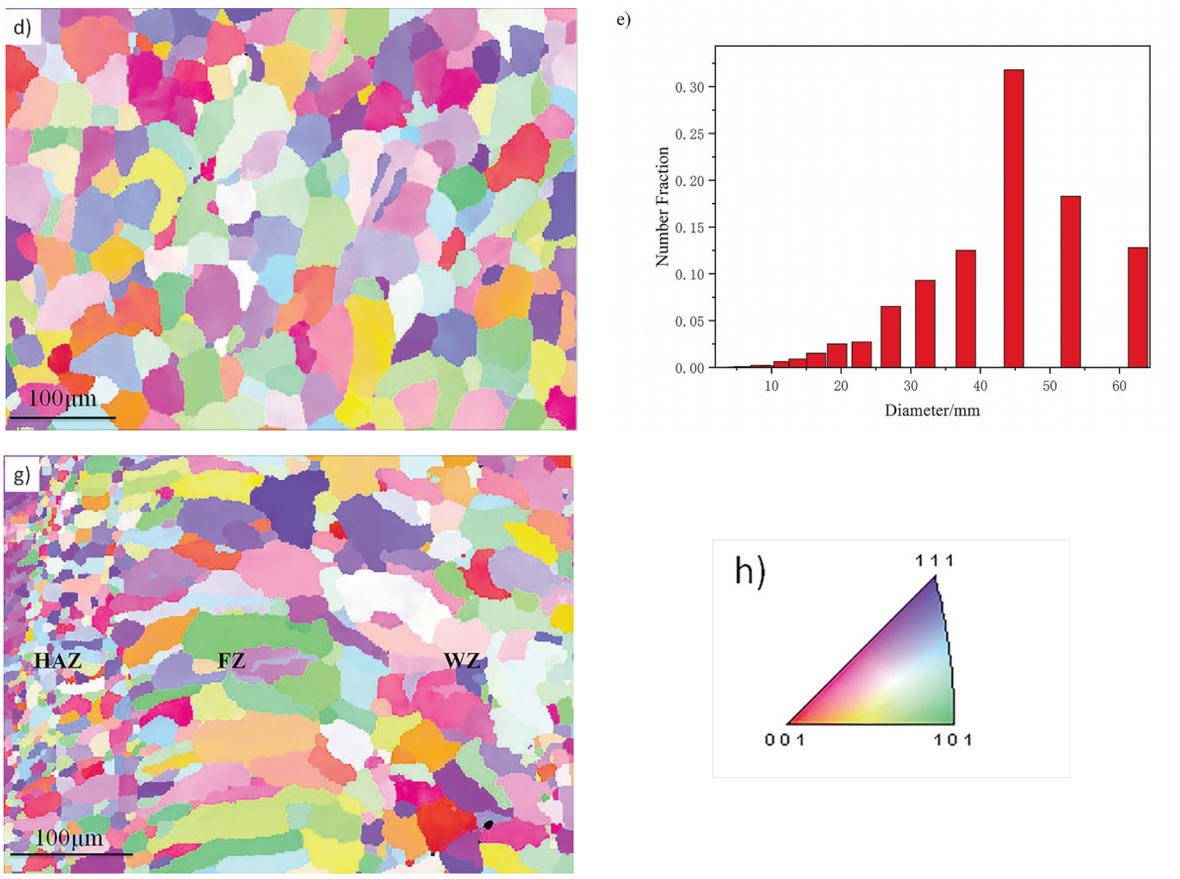


***Continued Figure 5.*** *7N01/5356 welded joint: d) weld zone, e) grain size distribution image of the weld zone, g) fusion zone; h) representation of the color code used to identify the crystallographic orientations on standard stereographic projection (red: [001]; blue: [111]; green: [101])*

visible in the weld zone of the 7N01/5087 welded joint (Fig. 7d). These particles were non-coherent with the matrix because the weld zone was as-cast structure.

For the molten metal in the weld zone during the welding process, the critical nucleation energy could be written by the following equation [22]:

$$\Delta G = (\frac{16\pi\sigma_{LS}^2}{3\Delta G_v}) \cdot (\frac{2-3\cos\theta+\cos^3\theta}{4}) \quad (1)$$

Where $\sigma_{LS}$ is the interface energy between liquid and solid; $\Delta G_V$ is the Gibbs free energy difference between liquid and solid per unit volume; $\theta$ is the wetting angle between nucleation and matrix, and

$$\cos\theta = \frac{\sigma_{LC}-\sigma_{SC}}{\sigma_{LS}} \quad (2)$$

where $\sigma_{LC}$ is the interface energy between basement and liquid, and $\sigma_{SC}$ is the interface energy between basement and solid.

Moreover, the nucleation equation is written as follows:

$$\eta = A\exp[\frac{B\sigma_{LS}^3}{(\Delta T)2T}] \quad (3)$$

Where $\Delta T$ is supercool, $T$ is absolute temperature of phase transition, and $A$, $B$ are both material-dependent constants.

From the equations (1, 2, 3), the wetting angle($\theta$) directly affected the heterogeneous nucleation; the nucleation ability was inversely proportional to the size of the wetting angle, and smaller wetting angle ($\theta$) meant less undercooling and stronger nucleation capability [23].

Meanwhile, the wetting angle was related to the interfacial tension between crystal nuclei and heterogeneous cores ($\sigma_{SC}$). The smaller the $\sigma_{SC}$ , the smaller the $\theta$ and the more conductive to heterogeneous nucleation . When the crystal surface structure of nuclei was more similar to that of heterogeneous core, the interface energy would be smaller during the nucleation process due to the interface coherent principle, and therefore heterogeneous nucleation occurred more readily [24].

In the present paper, for the Zr-added 5087 welding wire, the amount of Zr made the primary $Al_3Zr$ phase particles preferentially precipitated in the

melting metal of the weld zone during the solidification process because of the high melting point of $Al_3Zr$ (about 1577℃) [25]. These primary $Al_3Zr$ phases which were $DO_{23}$ tetragonal structure (a=0.4013nm, c=1.732nm) acted as ideal heterogeneous nuclei during the solidification of Al matrix and increased the nucleation rate because they had a high degree of similarity to the Al crystalline structure (Table 4) [26]. Hence, they could achieve the best grain refinement effect of weld zone.

In addition, the primary $Al_3Zr$ phases had obvious dispersion strengthening effect [27]. For the weld zone of 7N01/5087 welded joint, the strengthening mechanisms included dispersion strengthening, grain refinement strengthening and solution strengthening, but that of 7N01/5356 welded joint was only solution strengthening. Hence, the strength of Zr-added 7N01/5087 welded joint was higher than the strength of Zr-free 7N01/5356 welded joint (Fig.4).

The welded joint was composed of the weld zone, the fusion zone, the heat-affected zone and the base metal. The heat-affected zone could be further subdivided into the quenching zone and the softening zone [28]. Fig.8 showed the bright field TEM images of different regions of the welded joints. The microstructure of the base metal was fibrous tissues with partially recrystallized grains, and there were many micro-level primary crystal phases and nano-scale precipitation particles (η' phase) inside (Fig. 8a and b). Compared to base metal in Fig. 8(a), although the softening zone was still fibrous grain structure, the recrystallization proportion increased and the

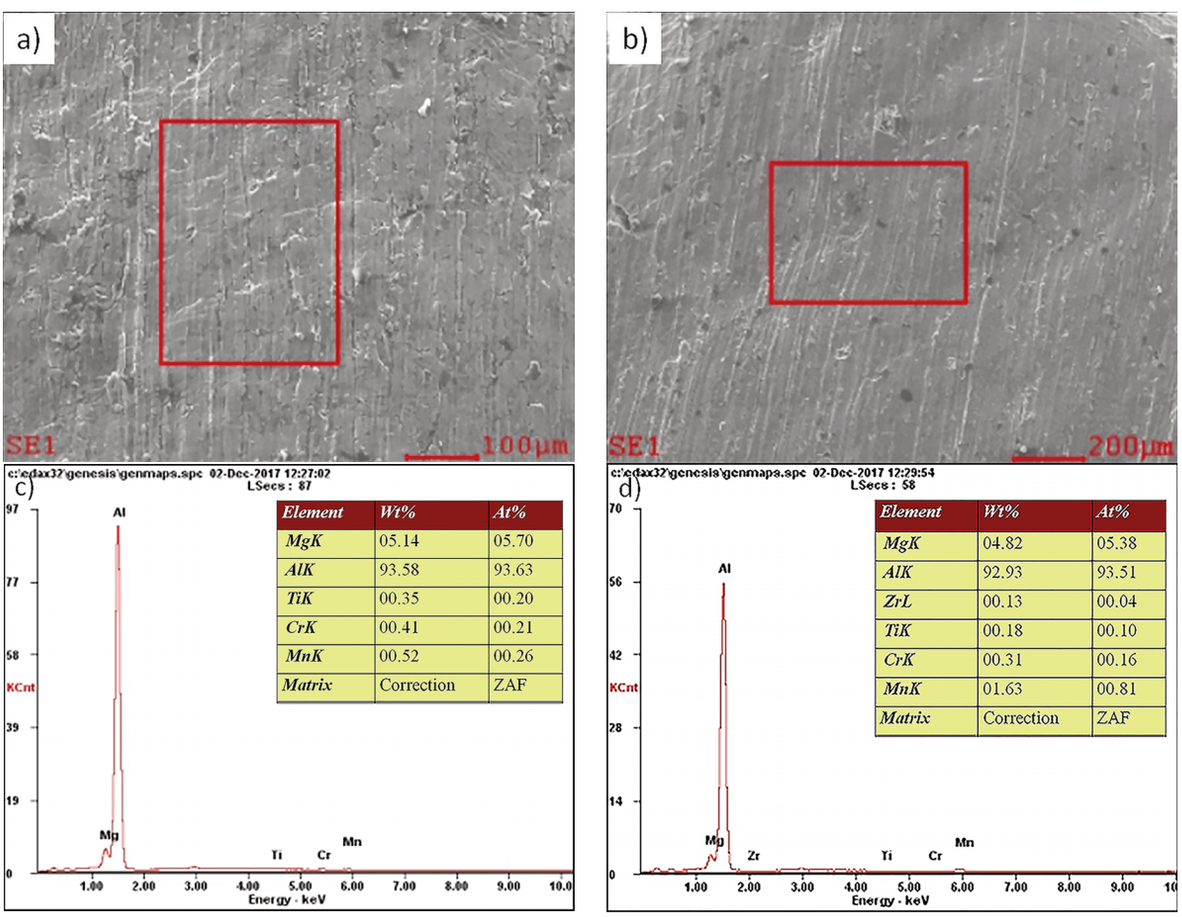


***Figure 6.*** *EDS results of the two weld zone: a, c) 7N01/5356 welded joint; b, d) 7N01/5087 welded joint*

***Table 4.*** *Lattice constant and crystal mismatch of $Al_3Zr$ and Al*

| | melting point/℃ | crystalline structure | lattice constant /nm | | crystal mismatch /% | |
|---|---|---|---|---|---|---|
| | | | a | c | $\delta_a$ | $\delta_c$ |
| Al | 660 | fcc | 0.405 | - | - | - |
| $Al_3Zr$ | 1577 | $LI_2$ | 0.408 | 0.408 | 0.99 | 0.99 |

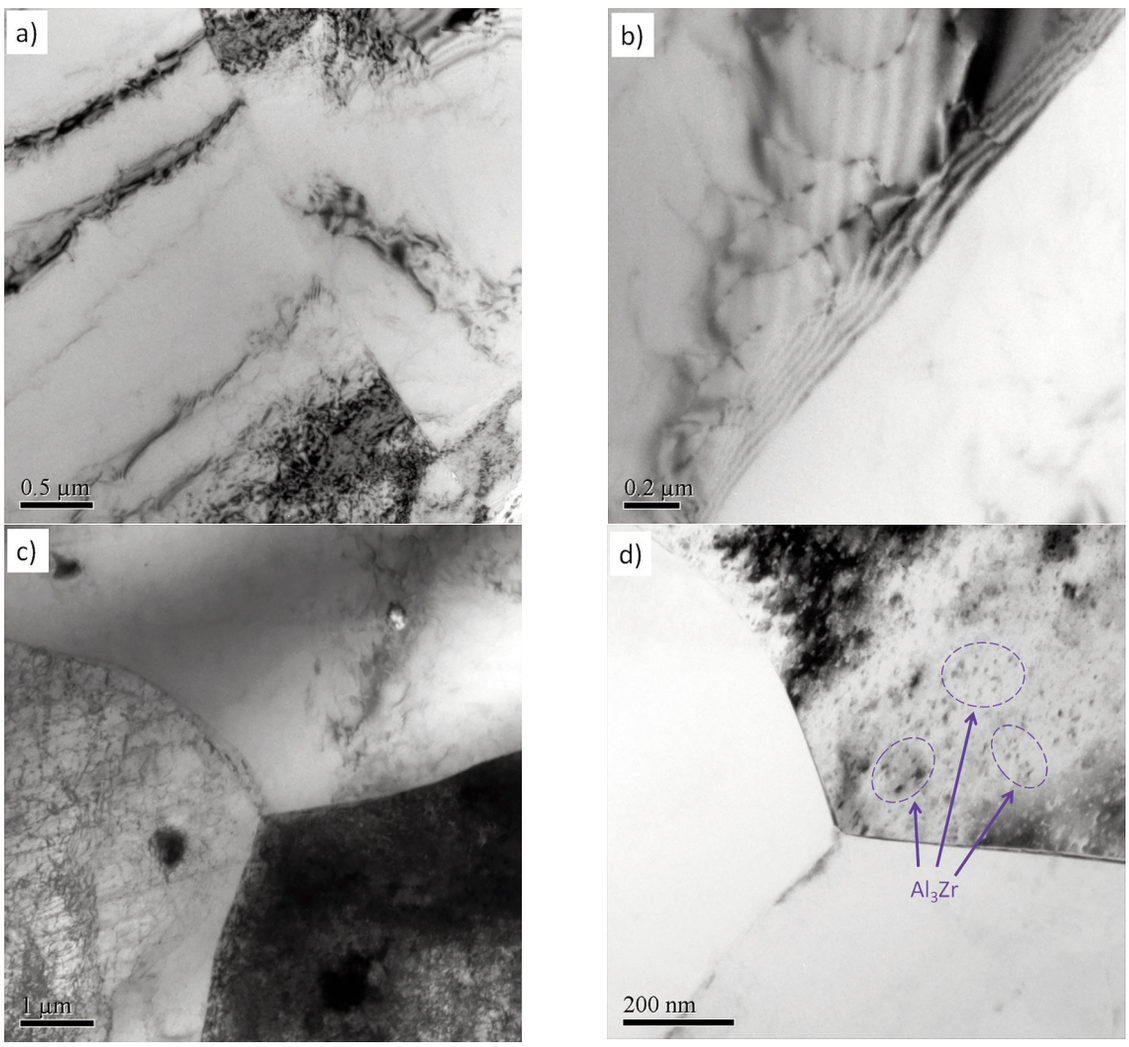


***Figure 7.*** *Bright field TEM images of weld zone of the two welded joints: a,b) 7N01/5356 welded joint, c,d) 7N01/5087 welded joint*

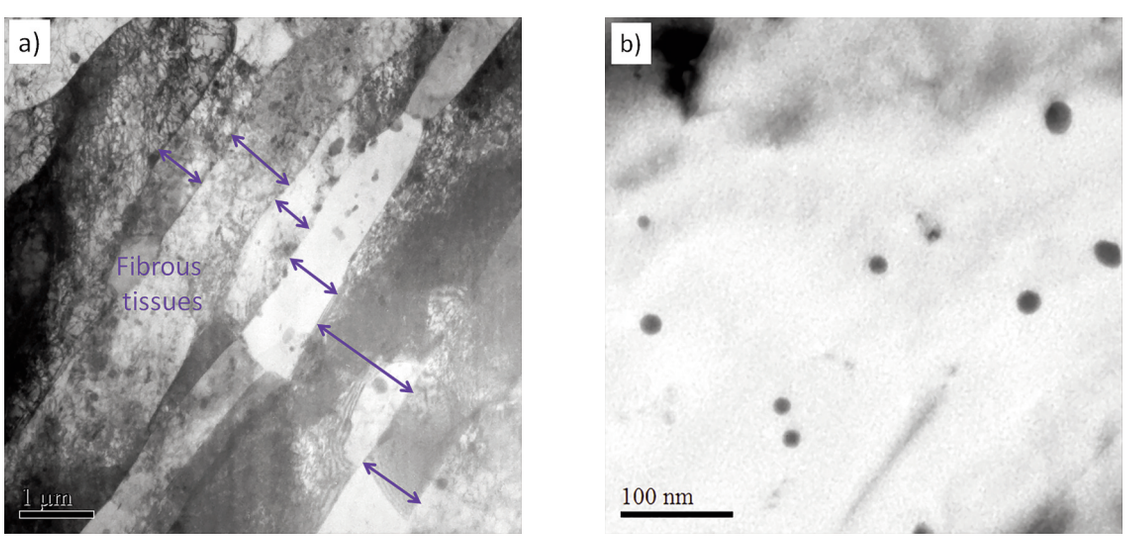


***Figure 8.*** *Bright field TEM images of different regions of the welded joints: a, b) base metal*

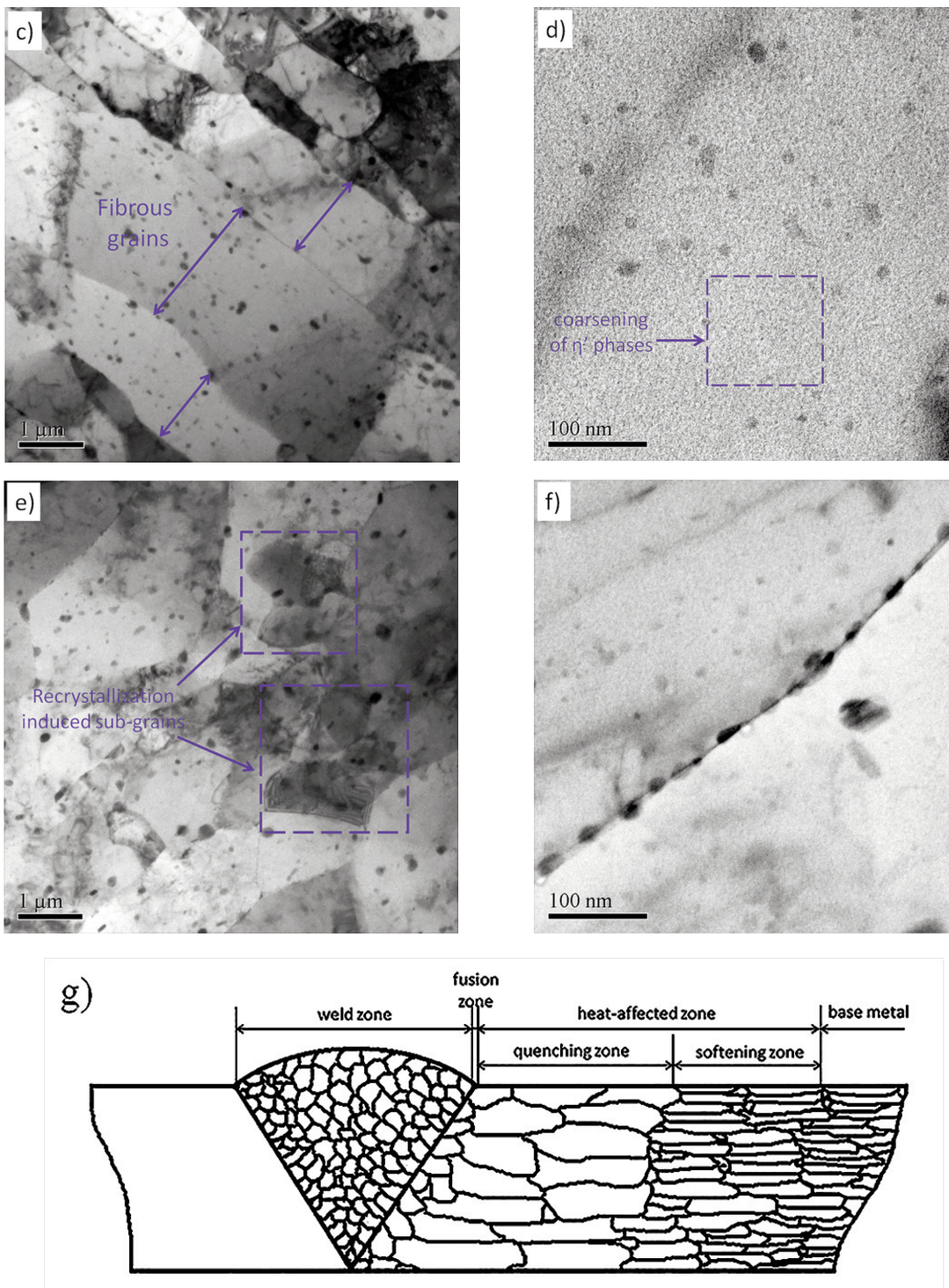


***Continued Figure 8.*** *c, d) softening zone, e, f) quenching zone g) schematic illustration of the welded joint*

elongated grains became wider (Fig. 8c). At high magnification, it could be seen that the precipitated phases were obviously coarsen (Fig. 8d). However, the fibrous grains and the precipitates in grains of the quenching zone disappeared (Fig. 8e and f). Moreover, the schematic illustration of the welded joint was shown in Fig. 8g.

## 4. Conclusions

In summary, ER5356 and ER5087 welding wires were employed to weld the 7N01-T5 Al alloy plates, and the mechanical properties and microstructures of the welded joints were investigated comparatively. Following conclusions could be drawn from the experimental results.

The joints welded by ER5087 weld wire exhibited higher properties compared with the 7N01/5356 welded sample;the ultimate strength and the elongation of 7N01/5087 welded joint were 320MPa and 6.4%, respectively, while those of 7N01/5356 welded joint were 288MPa and 4.9%, respectively.

The high strength and good elongation of 7N01/5087 welded joint was mainly attributed to the microstructure refinement in the weld zone through adding Zr element to promote the nucleation of Al grains around the $Al_3Zr$ sites.

### Acknowledgements

*The authors acknowledge the financial support by the National Natural Science Foundation of China (Grant No. 52004002).*

### Author's contributions

*Hu Xie: Performed the experiments and wrote the original draft; Lei Hu: Analyzed the results and revised the original draft; Qunshuang Ma: Performed the analysis with constructive discussions; Wei Meng: Data curation; Xiaohui Yin: Data curation.*

### Data Availability Statement

*The raw/processed data required to reproduce these findings cannot be shared at this time as the data also forms part of an ongoing study.*

### Conflict of interest statement

*The authors declare that they have no known competing financial interests or personal relationships that could have appeared to influence the work reported in this paper.*

### References

[1] I. Kovács, J. Lendvai, T. Ungar, G. Groma, J. Lakner, Mechanical properties of AlZnMg alloys, Acta Materialia, 28 (1980) 1621–1631. https://doi.org/10.1016/0001-6160(80)90015-2

[2] J. C. Williams, E. A. Starke Jr, Progress in structural materials for aerospace systems, Acta Materialia, 51 (2003) 5775–5799. https://doi.org/10.1016/j.actamat.2003.08.023

[3] T. Engdahl, V. Hansen, P. J. Warren, K. Stiller, Investigation of fine scale precipitates in Al-Zn-Mg alloys after various heat treatments, Materials Science and Engingeering A, 327 (2002) 59–64. https://doi.org/10.1016/S0921-5093(01)01876-7

[4] Q. Zhu, L. Chen, G. Zhu, X. Huo, Effect of Sc addition on low-cycle fatigue properties of extruded Al-Zn-Mg-Cu-Zr alloy, Materials Science and Technology, 36(1) (2020) 118-126. https://doi.org/10.1080/02670836.2019.1684668

[5] H. R. Zaid, A. M. Hatab, A. M. A. Ibrahim, Properties enhancement of Al-Zn-Mg alloy by retrogression and re-aging heat treatment, Journal of Mining and Metallurgy Section B:Metallurgy, 47 (1) B (2011) 31 – 35. https://doi.org/10.2298/JMMB1101031Z

[6] H. Xie, Z. Xiao, Z. Li, M. Wang, S. Ma, H. Jiang, Quench sensitivity of AA7N01 alloy used for high-speed train body structure, The Journal of The Minerals, Metals & Materials Society (TMS), 71(5) 2019 1681-1686. https://doi.org/10.1007/s11837-018-3162-z

[7] M. Pakdi, G. Çam, M. Koçak, S. Erim, Microstructural and mechanical characterization of laser beam welded AA6056 Al-alloy, Materials Science and Engineering A, 528 (2011) 7350–7356. https://doi.org/10.1016/j.msea.2011.06.010

[8] R. Kumar, U. Dilthey, D.K. Dwivedi, P.K. Ghosh, Thin sheet welding of Al 6082 alloy by AC pulse-GMA and AC wave pulse-GMA welding, Materials & Design, 30 (2009) 306-313. https://doi.org/10.1016/j.matdes.2008.04.073

[9] R. Manti, D.K. Dwivedi, A. Agarwal, Microstructure and hardness of Al-Mg-Si weldments produced by pulse GTA welding, International Journal of Advanced Manufacturing Technology, 36 (2008) 263-269. https://doi.org/10.1007/s00170-006-0849-z

[10] J. Górka, The assessment of the quality of welded joints made of abrasion-resistant plates using the nanocrystalline filler metal, Journal of Mining and Metallurgy Section B:Metallurgy, 56 (2) B (2020) 209–220. https://doi.org/10.2298/JMMB190515010G

[11] X. M. Wang, B. Li, M. X. Lia, H. G. Cui, H. Chen, Study of local-zone microstructure, strength and fracture toughness of hybrid laser-metal-inert-gas-welded A7N01 aluminum alloy joint, Materials Science and Engineering A, 688 (2017) 114–122. https://doi.org/10.1016/j.msea.2017.01.087

[12] K. Zhang, J. Q. Chen, P. Z. Ma, X. H. Zhang, Effect of welding thermal cycle on microstructural evolution of Al–Zn–Mg–Cu alloy, Materials Science and Engineering A, 717 (2018) 85-94. https://doi.org/10.1016/j.msea.2018.01.067

[13] A. K. Lakshminarayana, V. Balasubramanian, K. Elangovan, Effect of welding processes on tensile properties of AA6061 aluminium alloy joints, International Journal of Advanced Manufacturing Technology, 40 (2009) 286–296. https://doi.org/10.1007/s00170-007-1325-0

[14] I. B. Robinson, F. R. Baysinger, Welding Aluminum Alloy 7039, Welding Journal, 45 (1966) 433–444. https://doi.org/10.2351/1.5058333

[15] K. Shankar, W. D. Wu, Effect of welding and weld repair on crack propagation behaviour in aluminium alloy 5083 plates, Materials & Design, 27 (2006) 968-975. https://doi.org/10.1016/s0261-3069(01)00059-0

[16] B. Hu, I. M. Richardson, Mechanism and possible solution for transverse solidification cracking in laser

welding of high strength aluminium alloys, Materials Science and Engineering A, 429 (2006) 287–294. https://doi.org/10.1016/j.msea.2006.05.040

[17] Z. H. Zhao, Z. Xu, G. S. Wang, Effect of Sc, Zr, Er in ER5356 welding wire on mechanical properties of welded joint of 7A52 aluminum alloy, Chinese Journal of Materials Research, 27 (2013) 287-291. https://doi.org/CNKI:SUN:CYJB.0.2013-03-011

[18] X. F. Lei, Y. Deng, Y. Y. Peng, Microstructure and properties of TIG/FSW welded joints of a new Al-Zn-Mg-Sc-Zr alloy, Journal of Materials Engineering and Performance, 22 (2013), 2723-2729. https://doi.org/10.1007/s11665-013-0577-0

[19] L. Fu, Y. Y. Peng, J. W. Huang, Y. Deng, Z. M. Yin, Microstructures and mechanical properties of gas tungsten arc welded joints of new Al–Mg–Sc and Al–Mg–Er alloy plates, Materials Science and Engineering A, 620 (2015) 149–154. https://doi.org/10.1016/j.msea.2014.10.014

[20] J. W. Huang, Z. M. Yin, X. F. Lei, Microstructure and properties of 7A52 Al alloy welded joint, Transactions of Nonferrous Metals Society of China, 18 (2008) 804-808. https://doi.org/10.1016/S1003-6326(08)60139-9

[21] Y. Deng, B. Peng, G. Xu, Q. Pan, R. Ye, Y. Wang, L. Lu, Z. Yin, Stress corrosion cracking of a high-strength friction-stir-welded joint of an Al-Zn-Mg-Zr alloy containing 0.25 wt% Sc, Corrosion Science, 100 (2015) 57-72. https://doi.org/10.1016/j.corsci.2015.06.031

[22] S. Kou, Y. Le, Nucleation Mechanisms and grain refining of weld metal, Welding Journal, 65 (1986) 305–313. https://doi.org/10.1007/BF02628392

[23] G. D. Janaki Ram, T. K. Mitra, V. Shankar, S. Sundaresan, Microstructural refinement through inoculation of type 7020 Al–Zn–Mg alloy welds and its effect on hot cracking and tensile properties, Journal of Materials Processing Technology, 142 (2003) 174–181. https://doi.org/10.1016/S0924-0136(03)00574-0

[24] X. Z. Li, V. Hansen, J. Gjonnes, L. R. Wallenberg, HREM study and structure modeling of the η′ phase, the hardening precipitates in commercial Al-Zn-Mg alloys, Acta Materialia, 47 (1999) 2651–2659. https://doi.org/10.1016/s1359-6454(99)00138-x

[25] X. Y. Wei, H. Huang, Z. Y. Chen, W. Wang, C. Y. Li, Z. Y. Nie, Microstructure and mechanical properties of Al-Mg-Mn-Zr-Er weld joints filled with Al-Mg-Mn-Zr and Al-Mg-Mn-Zr-Er weld wires, Journal of Rare Earths, 28 (2010) 627-630. https://doi.org/10.1016/S1002-0721(09)60168-X

[26] Z. M. Yin, Yang. L, Q. L. Pan, Effect of minor Sc and Zr on microstructures and mechanical properties of Al-Zn-Mg based alloys, The Chinese Journal of nonferrous metals, 11 (2001) 822-825. https://doi.org/CNKI:SUN:ZYSY.0.2001-06-002

[27] Y. Deng, B. Peng, G.F. Xu, Q.L. Pan, Z.M. Yin, R. Ye, Y.J. Wang, L.Y. Lu, Effects of Sc and Zr on mechanical property and microstructure of tungsten inert gas and friction stir welded aerospace high strength Al–Zn–Mg alloys, Materials Science and Engineering A, 639 (2015) 500–513. https://doi.org/10.1016/j.msea.2015.05.052

[28] F. Matsuda, Effect of additional elements on weld solidification crack susceptibility of Al–Zn–Mg alloy, Report II, Transactions of the Japan Welding Research Institute, 12 (1983) 93–102. https://doi.org/10.1007/BF01447035

# MIKROSTRUKTURA I MEHANIČKE OSOBINE ZAVARENIH SPOJEVA A7N01 ALUMINIJUMSKE LEGURE ISPUNJENIH ER5356 I ER5087 ŽICAMA ZA VARENJE

**H. Xie *, L. Hu, Q.-H. Ma, W. Meng, X.-H. Yin**

Fakultet za nauku o materijalima i inženjerstvo, Tehnološki univerzitet Anhui, Maanšan, Anhui, Kina

***Apstrakt:***

*Ploče od legure aluminijuma A7N01-T5 debljine 12 mm zavarene su ER5356 i ER5087 žicama za zavarivanje metal inertni gas (MIG) postupkom. Mehaničke osobine i mikrostruktura zavarenih spojeva ispitivani su uz pomoć merenja mikro tvrdoće, zatezne čvrstoće, energetske disperzivne spektroskopije (EDS), elektronske difrakcije povratnim raspršenjem elektrona (EBSD) i transmisione elektronske mikroskopije (TEM). Rezultati su pokazali da su zatezna čvrstoća i izduženje zavarenih spojeva 7N01/5087 (ploča od legure aluminijuma 7N01 zavarena ER5087 žicom) bili veći nego kod 7N01/5356 zavarenih spojeva (ploča od legure aluminijuma 7N01 zavarena ER5356 žicom). Visoka čvrstoća i dobro izduženje zavarenog spoja 7N01/5087 uglavnom se pripisuje mikrostrukturnoj rafinaciji u zoni zavarivanja dodavanjem Zr elementa da bi se poboljšala nukleacija Al zrna oko $Al_3Zr$ mesta.*

***Ključne reči:*** *Legure aluminijuma; ER5087 žica za zavarivanje; ER5356 žica za zavarivanje; Mikrostruktura; Mehaničke osobine*